

# Numerical Simulation of Fire-Smoke Diffusion Caused by Vehicles in a Tunnel

Li Lei\*, Wukai Chen, Huiling Li and Shuai Shi

School of Energy and Power Engineering, Shandong University, Jinan, China

\*Corresponding Author: Li Lei. Email: leili@sdu.edu.cn

Received: 10 January 2020; Accepted: 04 August 2020

**Abstract:** Urban tunnels are generally narrow and fire smoke can hardly diffuse. In the present study, numerical simulation is used to analyze the diffusion of high temperature smoke produced by fire inside a specific tunnel (the Kaiyuan tunnel). The results are compared with similar data relating to other tests to determine the validity of the numerical method. Moreover, the critical velocity obtained by numerical simulation of 5 MW, 20 MW, and 50 MW fires in curved and linear sections of the considered tunnel is compared with the values obtained using empirical formulas. The results show that, for the tunnel ventilation design, it is necessary to consider the fan pressurization at different sections and the fan pressurization should be higher at curved sections than that at linear sections. The safety of personnel escaping under different critical velocity values in the linear section has also been considered. On the basis of our findings, if only relying on natural ventilation, people can escape safely for the case of small fires, whereas for medium and large fires, it is necessary to turn on mechanical ventilation in time (and in order to avoid the danger caused by rapid diffusion of smoke, the timing of mechanical ventilation should be carefully tuned).

**Keywords:** Numerical simulation; critical velocity; smoke diffusion; personnel escape preparation

## 1 Introduction

In recent years, as the pace of urban modernization continues to increase, urban traffic congestion has become a common phenomenon. More and more cities have begun to build urban tunnels to improve traffic conditions. A tunnel is an enclosed, narrow, and long space. During a fire accident, under the action of tunnel ventilation, the high-temperature, high-concentration, and low-visibility toxic smoke released by the fire will spread rapidly along the tunnel, posing a threat to people, vehicles, equipment, and structures in the tunnel. In the past 20 years, many studies have been conducted on the diffusion characteristics of tunnel fire smoke by means of experiments and numerical simulations.

The Offenegg tunnel fire experiment in 1965 was the first experiment to investigate fire development and smoke flow under different ventilation conditions [1]. In 1989, the research institute of the Guangzhou Railway Bureau conducted a 1:3 section simulation test in the training tunnel of the rescue team of the Sichuan Huakinshan Mining Bureau. The test proved that it was effective to put out the fire using the block-end oxygen suffocation method when a fire breaks out in a tunnel [2]. In 2004, Bari et al. [3] used



This work is licensed under a Creative Commons Attribution 4.0 International License, which permits unrestricted use, distribution, and reproduction in any medium, provided the original work is properly cited.

FLUENT to simulate the smoke pollution caused by burning buses during congestion in an urban connection tunnel. They concluded that the evacuation time was 6–8 min after the start of combustion, so there should be a quick evacuation channel in a tunnel. In the same year, Hu et al. [4] conducted a comprehensive combustion test in a corridor to study the changes in the smoke temperature and velocity, and the results showed that the temperature decreased exponentially with distance.

With the development of computer technology, Computational Fluid Dynamics (CFD) has become an important means of academic research, and numerical simulation methods have been widely used in the study of fluid dynamics [5–9]. Currently, studying the fire-smoke behavior using numerical simulations is a popular research topic. Dobashi et al. [10] from Japan used a computational fluid dynamics (CFD) method to study emergency ventilation in a tunnel fire and applied the results to the high-speed Dongshan tunnel in Nagoya, which was under construction. Demouge and Lacroix of Japan [11] used CFD to calculate the flow of fire smoke under transverse ventilation. Levy et al. [12] of the United States used the SOLVENT CFD software to improve the operation mode matrix for emergency ventilation of the Ted Williams tunnel and discussed the relationship between the exhaust air volume and the smoke control effect in a tunnel fire. Yao [13] used the FLUENT software to numerically simulate the distribution of the temperature field under different ventilation velocities and fire sizes. Wu et al. [14] used the large eddy simulation method to numerically study the fire smoke spreading behavior of a highway tunnel with a small-radius curve. Wu [15] built a three-dimensional mathematical model of a tunnel fire based on turbulent combustion theory and analyzed the structural safety during the tunnel fire by combining numerical simulations with physical tests. Hua et al. [16] explored the basic parameters, the tunnel model mesh generation, the fire source parameters, the smoke control and exhaust parameters, and the vehicle evacuation downstream of the fire source using a numerical simulation of a tunnel vehicle fire. Cao [17] studied the frequently congested Eight Scenic Mountain Highway Tunnel using fire dynamics simulator (FDS) software that considered the traffic tunnel fire conditions, the traffic congestion, and the evacuation of people as well as the relationship between them.

In this study, using the volume heat source (VHS) method to simulate a tunnel fire reported previously, it was concluded that a FLUENT model was useful for analyzing tunnel fire disasters with the appropriate parameters. Small, medium, and large fires in the linear and curved sections of a tunnel were simulated, the critical velocity was obtained, the safety of people evacuating the tunnel was evaluated, and guidelines for the use of ventilation after the fire starts were determined. The results of this study have important reference value for the traffic operation of general tunnels and the emergency treatment of unexpected accidents in tunnels.

## 2 Mathematical Model

### 2.1 Governing Equations

The distribution of flow field in tunnel under fire condition follows three basic principles of physics: the law of conservation of mass, the law of conservation of momentum and the law of conservation of energy. In this study, the fire source was regarded as a fixed point source. It is assumed that the fluid is an incompressible fluid with constant physical properties, and the flow field is simulated by solving the Navier-Stokes equation.

The mass equation, the momentum equation and energy equation are as follows:

$$\frac{\partial u_i}{\partial x_i} = 0 \quad (1)$$

$$\rho \frac{\partial}{\partial x_j} (u_i u_j) + \rho \frac{\partial u_i}{\partial t} = - \frac{\partial p}{\partial x_i} + \frac{\partial \tau_{ij}}{\partial x_j} + \rho g_i \quad (2)$$

$$\frac{\partial(\rho T)}{\partial t} + \text{div}(\rho u T) = \text{div}\left(\frac{\lambda}{C_p} \text{grad} T\right) + S_T \quad (3)$$

where  $u$  is the velocity;  $p$  is static pressure;  $\rho$  is the density;  $\tau_{ij}$  is stress tensor;  $\rho g_i$  is gravity volume force.  $C_p$  means heat capacity;  $T$  is temperature;  $\lambda$  is the heat transfer coefficient of the fluid;  $S_T$  is the internal heat source of a fluid.

The governing equations (k- $\varepsilon$  equation and component transport equation) in the solving process are as follows:

$$\frac{\partial}{\partial t}(\rho k) + \frac{\partial}{\partial x_i}(\rho k u_i) = \frac{\partial}{\partial x_j} \left[ \left( \mu + \frac{\mu_t}{\delta_k} \right) \frac{\partial k}{\partial x_j} \right] + G_k + G_b - \rho \varepsilon - Y_m + S_k \quad (4)$$

$$\frac{\partial}{\partial t}(\rho \varepsilon) + \frac{\partial}{\partial x_i}(\rho \varepsilon u_i) = \frac{\partial}{\partial x_j} \left[ \left( \mu + \frac{\mu_t}{\delta_\varepsilon} \right) \frac{\partial \varepsilon}{\partial x_j} \right] + \rho C_1 S_\varepsilon - \rho C_2 \frac{\varepsilon^2}{k + \sqrt{V_\varepsilon}} + C_{1\varepsilon} C_{3\varepsilon} G_b \frac{\varepsilon}{k} + S_\varepsilon \quad (5)$$

$$\frac{\partial}{\partial t}(\rho Y_i) + \frac{\partial}{\partial x_j}(\rho v Y_i) = - \frac{\partial}{\partial x_j}(J_i) + S_i \quad (6)$$

where  $k$  and  $\varepsilon$  are the turbulent kinetic energy and turbulence dissipation rate,  $\mu$  and  $\mu_t$  is the viscosity and dynamic viscosity,  $G_k$  is the turbulent kinetic energy of the average velocity gradient,  $G_b$  is the turbulent kinetic energy generated by buoyancy, and  $Y_m$  is the contribution of pulsating expansion of compressible turbulence to the total dissipation rate.  $C_1$ ,  $C_2$ ,  $C_{1\varepsilon}$  and  $C_{3\varepsilon}$  are constants,  $\delta_k$  and  $\delta_\varepsilon$  are turbulent Prandtl Number for  $k$  and  $\varepsilon$  and  $S_k$  and  $S_\varepsilon$  are custom source terms.  $Y_i$  is the mass fraction of substance  $i$ ,  $S_i$  is some rate of formation of substance  $i$ ,  $J_i$  is the mass diffusion flux of substance  $i$ .

To solve natural convection problems in non-isothermal flows, the Boussinesq model was used. It has better convergence than defining the density as a function of temperature. The approximate basis of the model is that the temperature change range is small, and the density change is not obvious. This model only considers the dependence of density on temperature for the production term at the right hand side of the momentum balance equation, and the density is considered to be a constant when solving other equations.

## 2.2 Boundary Conditions

- (1) Initial conditions. The initial temperature was set as 293.15 K and was evenly distributed. The air density was 1.225 kg/m<sup>3</sup>, the specific heat capacity at constant pressure was 1006.43 J/(kg·K), and the thermal expansion coefficient for an ideal gas is the inverse of the absolute temperature, i.e., 0.0034 K<sup>-1</sup>. The thermal conductivity of the air was 0.0242 W/(m·K), and the viscosity coefficient was 1.7894 × 10<sup>-5</sup> kg/(m·s). The standard k- $\varepsilon$  turbulence model was used.
- (2) Entrance boundary conditions. When there was no longitudinal ventilation in the tunnel, the tunnel entrance was set as a pressure inlet, and when there was longitudinal ventilation, a velocity inlet was used.
- (3) Exit boundary conditions. The tunnel exit was set as a pressure outlet.
- (4) Wall boundary conditions. To reduce the calculation time, the walls were set as adiabatic walls.

## 2.3 Physical Model

A simplified vehicle body of different models was selected, and the exhaust pipe was simplified as a single round hole at the rear of the vehicle.

### 2.3.1 Car

The car studied in this paper was the Notchback MIRA model, whose three views and dimensions are shown in Fig. 1 and Tab. 1. Abundant test data have been previously collected for this model, and it has been widely used as a simplified automobile body model [18,19].

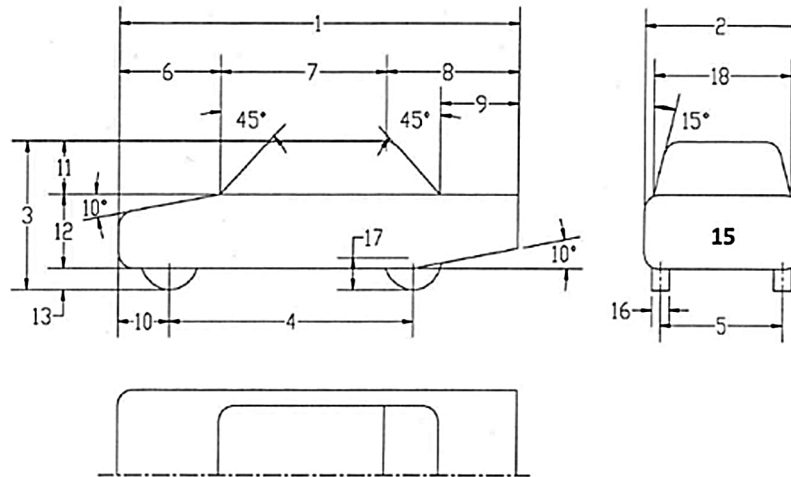


**Figure 1:** Notchback MIRA model

**Table 1:** Dimensions of the Notchback MIRA model

Label	1	2	3	4	5	6
Size (mm)	4165	1625	1420	2540	1270	1055
Label	7	8	9	10	11	12
Size (mm)	1790	1320	750	535	508	708
Label	13	14	15	16	17	18
Size (mm)	205	152	1.856	180	305	1420

The Notchback MIRA model was created with the PRO/Engineering software, and its tire positions were set. The tire contact position with the ground was set as a plane, and the exhaust pipe was modeled as a round hole with a diameter of 0.04 m in the lower right corner of the rear of the car, 0.4 m from the ground. The car model used for the subsequent analysis is shown in Fig. 2.

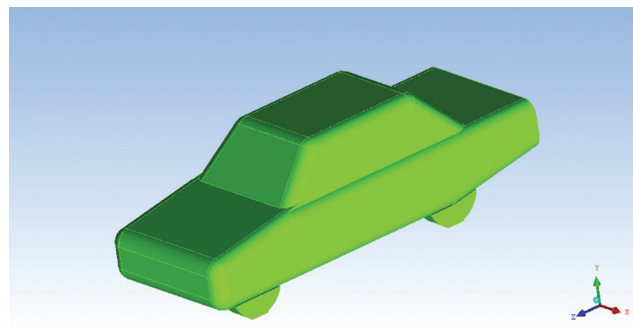


**Figure 2:** Three-dimensional view of car model

### 2.3.2 Truck

Li et al. [20,21] performed CFD simulations to study the aerodynamic characteristics of a truck under different working conditions and obtained many results. The size of the truck used in this study was selected based on their model. The exhaust pipe was modeled as a round hole with a diameter of 0.06 m in the middle of the back of the truck, 0.7 m from the ground, as shown in Fig. 3.

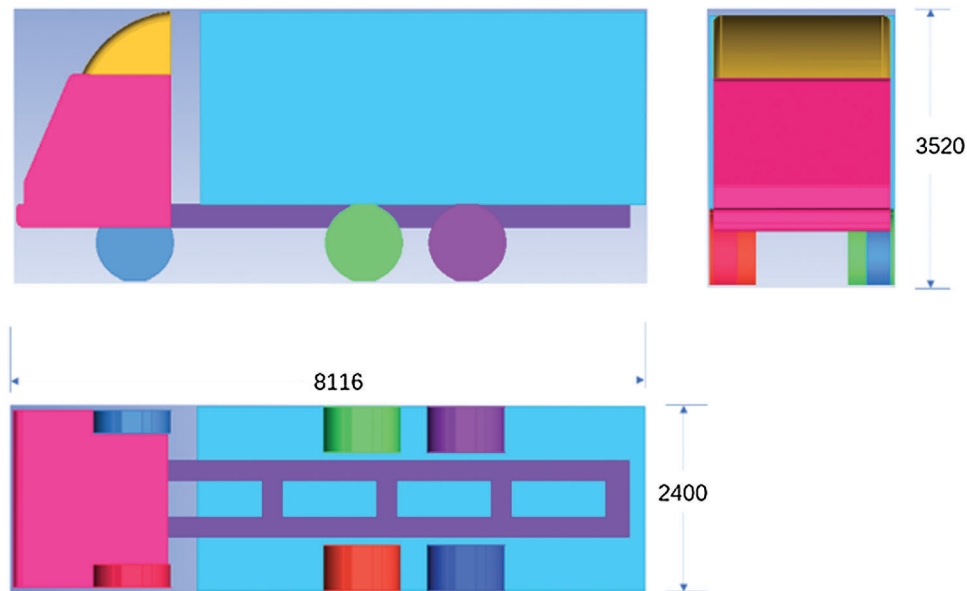


**Figure 3:** Truck model and dimensions

### 2.3.3 Bus

The most common type of bus is 10-m long. Thus, the size of the bus selected in this study was 10 m × 2.5 m × 3 m, as shown in Fig. 4.

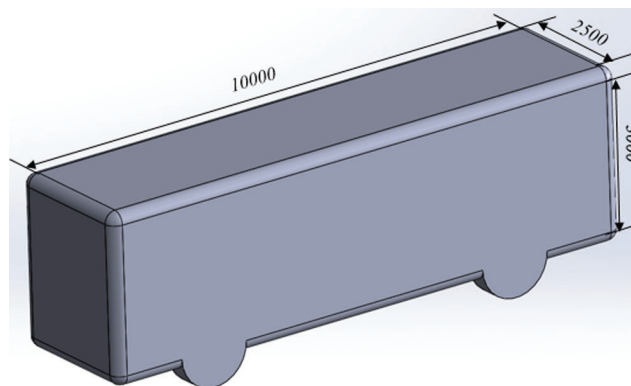


**Figure 4:** Bus model and dimensions

### 2.3.4 Curved and Linear Sections of the Tunnel

The overall top view of the north tunnel of the tunnel is shown in Fig. 5. There were jet fans 200 m from the north tunnel entrance, and 200 and 350 m from the exit. Each group contained two sets of jet fans; there

was a total of six sets. The tunnel ventilation mode was longitudinal ventilation. The ventilation was natural when the fan was closed and mechanical after the fan was opened.

The linear section in the middle of the north tunnel was selected for this study, as shown in Fig. 5. This section is highlighted by the red box in Fig. 5 and had a length of about 300 m. The radius of curvature was  $R = 600$  m in the curved region near the tunnel entrance. This section is highlighted by a blue box in Fig. 5 and had a length of 400 m. The geometric models of the linear and curved segments are shown in Figs. 6 and 7.

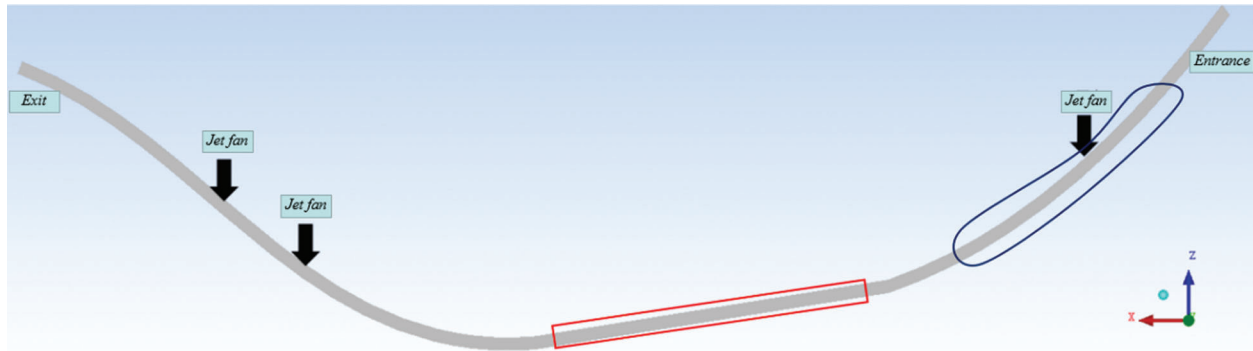


**Figure 5:** Overall top view of the North tunnel of the Tunnel

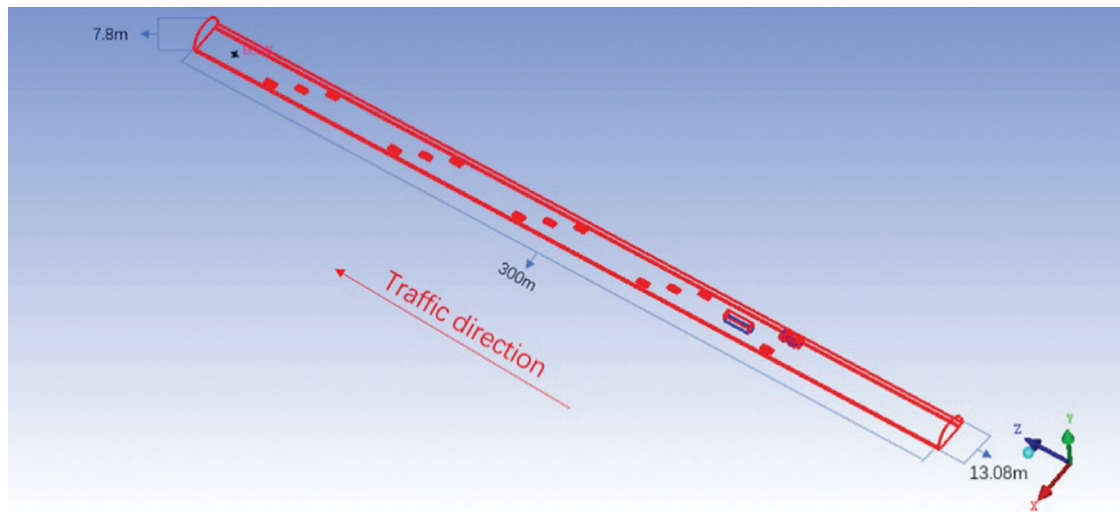


**Figure 6:** Geometric model of linear segment

### 2.3.5 Jet Fan

The structure of the jet fan used in the tunnel is shown in Fig. 8. The height at the center of the fan was  $h = 6$  m, the diameter of the fan blade was  $D = 1$  m, and the overall length was  $L = 5$  m. The outer surface of the fan was set as a wall, and the air outlet of the fan was set as interface in the numerical simulations. The layout of the jet fan is shown in Fig. 9.

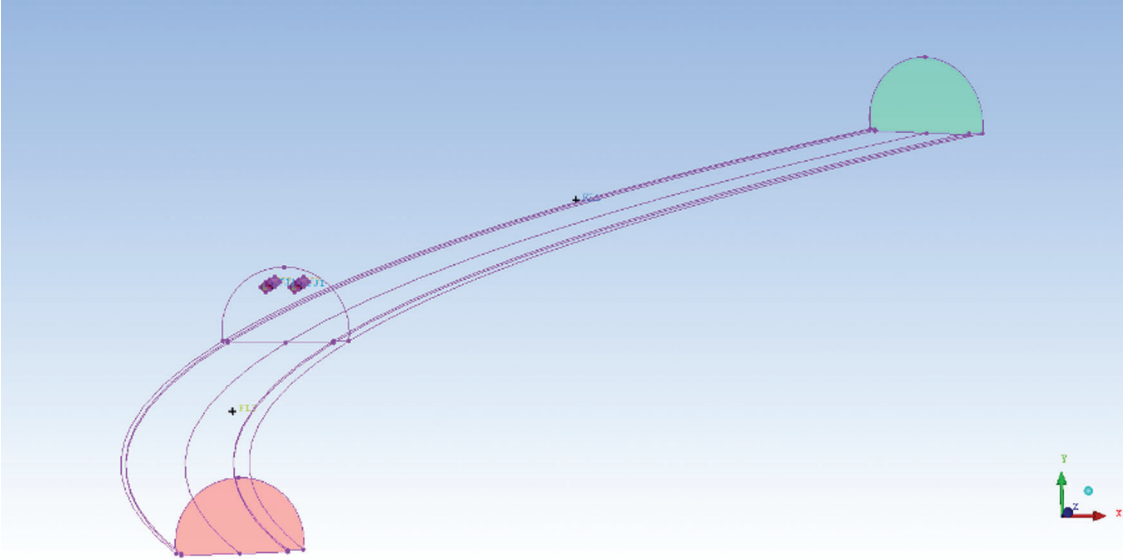


Figure 7: Geometric model of curved segment

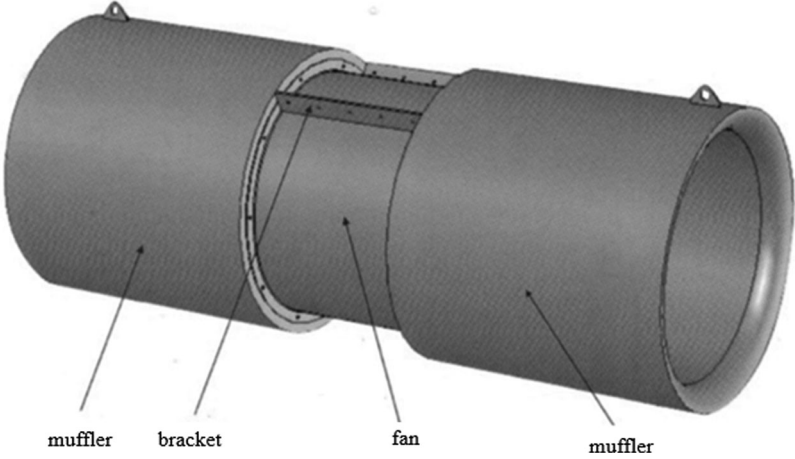


Figure 8: Structure of the jet fan

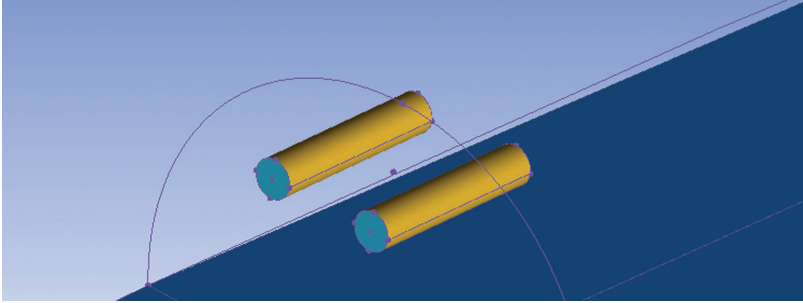
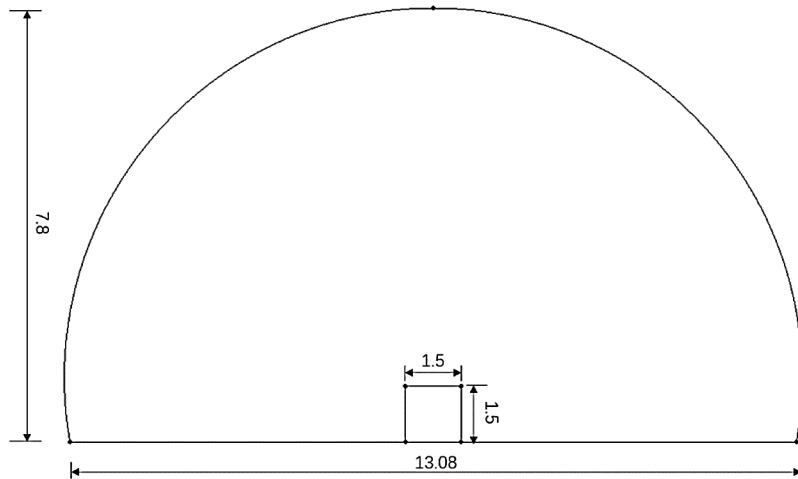


Figure 9: Layout of the jet fan

### 2.4 Mesh Division

To facilitate the modeling and mesh division, the tunnel was simplified appropriately. The linear and curved segments described above were used in the simulation of a single car fire. The tunnel section was taken as an arch, and the left and right sidewalks were removed. The tunnel contour was treated as the curve of a circle, and the fire sources were simplified as rectangular cuboids. The fire source size was  $1.5 \text{ m} \times 1.5 \text{ m} \times 4 \text{ m}$ . The tunnel section and fire source models are shown in Fig. 10.



**Figure 10:** Tunnel section and fire source models

A regular hexahedral mesh was adopted for the calculations, and the calculation domain of the tunnel air flow field and the mesh of the fire source was created. In FLUENT, the fluid flow and heat transfer coupling was carried out using the APPEND option. Because the temperature and flow fields change dramatically near the fire source, the mesh was refined near the fire point. The mesh size reached 2 million cells, and the mesh mass was above 0.9, as shown in Fig. 11.

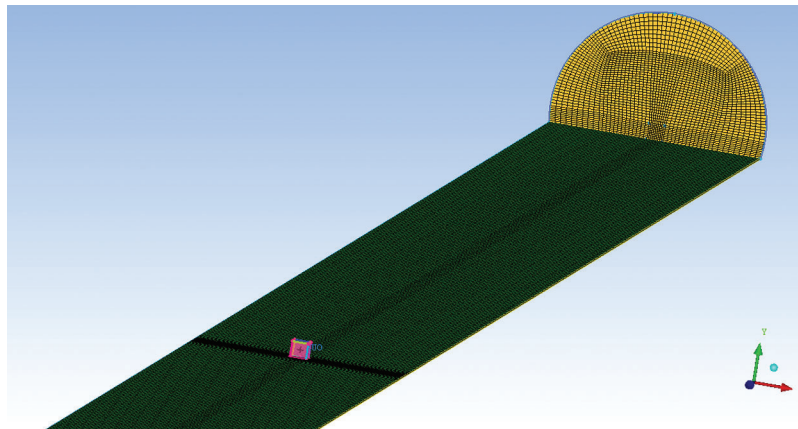


**Figure 11:** Mesh division

### 3 Numerical Method

In this study, the  $k-\varepsilon$  double equation turbulence model with buoyancy correction, the finite volume heat source (VHS) combustion model, the discrete ordinates (DO) radiation model and the component transfer equation were used, and the pressure correction method of PRESTO was used to solve the discrete equations. The VHS model is the simplest combustion model [22,23]. It sets the heat source as a fixed volume heat source of limited size to study the influence of the combustion process of the fire source on the flue gas flow and temperature field. The basic idea of the DO radiation model is to discretize the space radiation heat transfer in multiple directions and calculate the change of the medium absorption and scattering coefficients in space coordinates (x, y, z) [24,25]. The calculation result is closer to the actual situation. The PRESTO method calculates the interlaced pressure of the interlaced control grid by discretizing the continuous equilibrium equation [26,27].

#### 3.1 Basic Assumptions

To simplify the complex tunnel fire smoke diffusion problem, the following assumptions were used.

- (1) Before the fire, the air temperature distribution in the tunnel is uniform and the air flow is turbulent.
- (2) The tunnel wall is adiabatic, and no heat exchange is considered at the walls of the concrete structure.
- (3) The gas flow in the tunnel and the smoke generated by the fire are regarded as a multi-component ideal gas that obeys the ideal gas equation of state.
- (4) Chemical changes in the high-temperature smoke in the tunnel are ignored.

#### 3.2 Fire Source Setting

In this study, the volume heat source method (VHS) was adopted, i.e., the fire source was regarded as a fixed heat source based on the heat released by the fire, and the full combustion stage of the fire was studied by means of a steady-state fire source.

#### 3.3 Verification of Numerical Calculation Method

To validate the model adopted in this study, a simulation using a set of working conditions in the Memorial Tunnel Fire Ventilation Test Program (MTFVTP) in the United States was performed [28]. Fig. 12 shows a schematic diagram of the cross section of the tunnel, with the rectangular part at the bottom as the road and the semicircular part at the top as the ventilation duct. The VHS method was adopted to simulate the ventilation conditions in the case of fire in the tunnel using FLUENT.

The fire scale was selected based on test condition No. 502 in the test scheme (i.e., the fire scale was 10 MW). Two jet fans were opened 5 min after the fire started. Figs. 13a and 13b show the velocity and temperature distributions, respectively, 66 m downstream from the fire source. Based on the locations of the temperature and speed sensors in the test, the velocity and temperature distributions of the center line of the section at heights of 0.3, 1.2, 2.4, 3.6, 4.8, 5.7, 6.5, and 7.3 m were selected.

Fig. 13 shows that the temperature distribution obtained by the numerical simulation was basically consistent with the test results. However, the predicted temperatures in the middle positions of the tunnel section were slightly larger than the measured temperatures, which was similar to the numerical result obtained by Martegani et al. [29]. In the middle section of the tunnel, the velocity distribution of the numerical calculation was consistent with the experimental results. However, the numerical results at the upper and lower sections near the wall were slightly larger than the experimental results. This may have been because wall heat transfer was not considered in the numerical calculation, and the heat distribution difference caused by convection and conduction in the area close to the wall was more significant. Consequently, the fire ventilation pressure drove the air flow more forcefully, and the speed was higher than the experimental value.

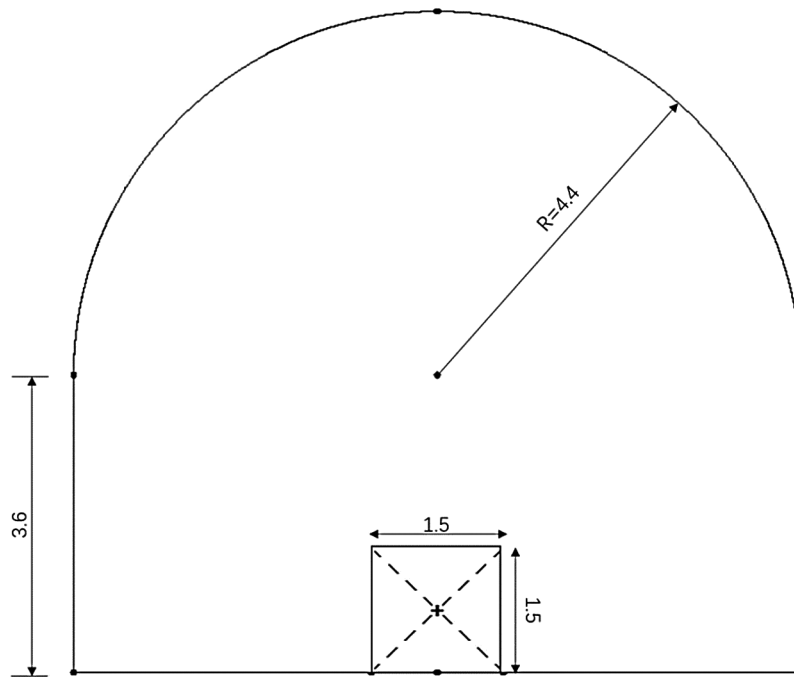


**Figure 12:** Cross section of the tunnel

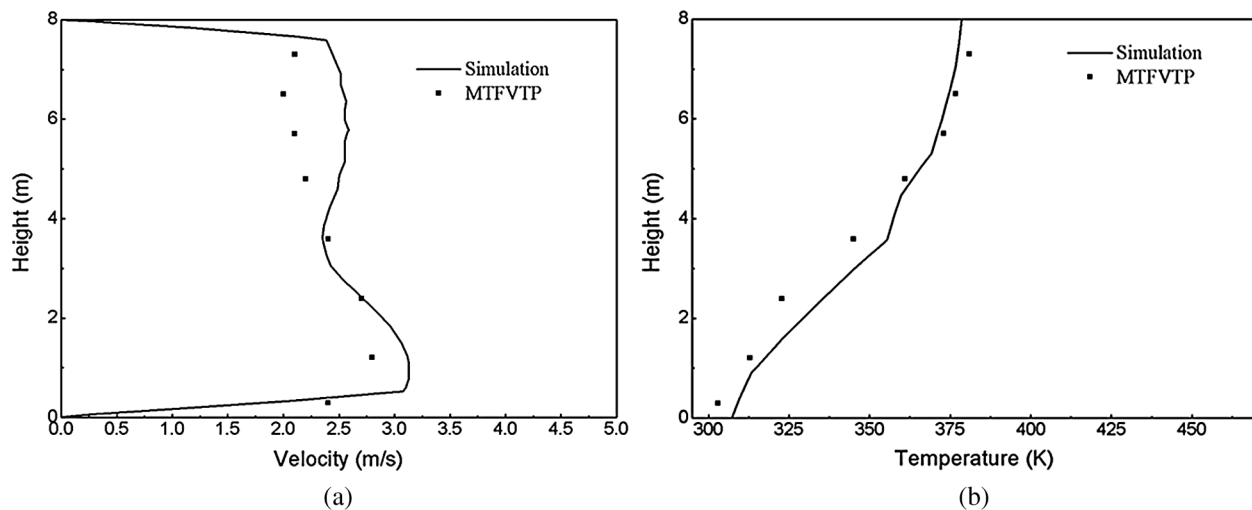


**Figure 13:** Temperature and velocity distributions on the center line 66 m downstream from the fire source. (a) Velocity distribution and (b) Temperature distribution

The above analysis results show that the numerical and experimental results were in good agreement, which indicated that the numerical model and method adopted in this paper were reasonable.

## 4 Results and Analysis

### 4.1 Mesh Independence

The size and number of computational nodes will affect the results of numerical calculations, including velocity and temperature distribution. The influence of mesh refinement was studied. Taking the inflow velocity at the same

position in front of the truck with a complex model structure as the monitoring object, the calculation results of the inflow velocity with different mesh numbers were compared. The results are shown in the Tab. 2.

As can be seen from the Tab. 2, when the number of computational nodes is 1.8 million and 2.4 million, there is a small difference in the calculation results. It can be considered that when the number of computational nodes is greater than 1.8 million, the calculation results have nothing to do with the number of computational nodes. In order to ensure the accuracy of calculation result, the number of computational nodes divided in this research is greater than 2 million. The mesh diagram and monitoring point of the truck model are shown in Fig. 14.

**Table 2:** Mesh sensitivity analysis

Mesh size (million)	0.6	1.2	1.8	2.4
The inflow velocity of the monitoring point (m/s)	16.25	18.51	20.14	21.44

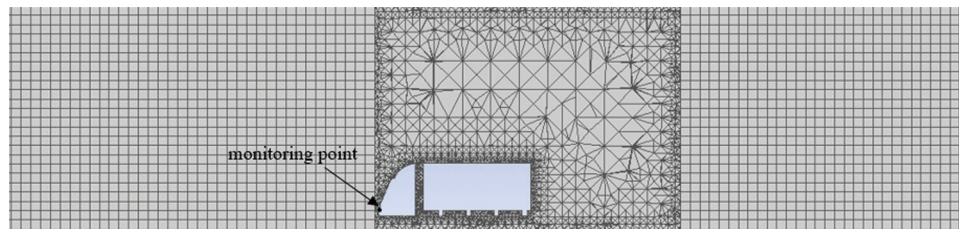


**Figure 14:** Mesh diagram and Monitoring point of the Truck model

#### 4.2 Critical velocity

The critical velocity is the key to controlling tunnel smoke. It is the minimum longitudinal ventilation velocity that can effectively prevent the smoke from traveling downwind of the fire source without an adverse flow. Many studies on the critical velocity have been conducted [30–32]. In general, the critical velocity can be calculated by the Heselden & Kennedy formula [33]:

$$v_c = k_g \cdot k \left( \frac{gHQ_w}{\rho C_p A T_f} \right)^{1/3} \quad (7)$$

$$T_f = T + \frac{Q_w}{\rho C_p A v_c} \quad (8)$$

where  $v_c$  is the critical velocity (m/s);  $k_g$  is the slope correction factor [34], where the level slope and the upper slope were 1.0 in this model, and the grade is the tangent value corresponding to the tunnel slope expressed as a percentage;  $k$  is the dimensionless coefficient,  $k = 0.61$ ;  $g$  is the gravitational acceleration,  $9.81 \text{ m/s}^2$ ;  $H$  is the clearance height of the tunnel section (m);  $Q_w$  is the heat release rate of the fire source, (kW);  $\rho$  is the air density,  $1.225 \text{ kg/m}^3$ ;  $C_p$  is the specific heat capacity at constant pressure,  $1006.43 \text{ J/(kg}\cdot\text{K)}$ ;  $A$  is the ventilation area of the tunnel ( $\text{m}^2$ );  $T_f$  is the smoke temperature (K); and  $T$  is the ambient air temperature,  $293.15 \text{ K}$ .

The tunnel height  $H$  was  $7.8 \text{ m}$ . The tunnel bottom was flat, so the slope correction factor  $k_g$  was  $1.0$ . The net fault surface area of the tunnel,  $A$ , was calculated to be  $69.1353 \text{ m}^2$ . Based on the literature and specifications (Tab. 3) [35], the heat release rate  $Q_w$  of the fire source was  $5$ ,  $20$ , or  $50 \text{ MW}$  based on the fire size. The critical velocities of the small, medium, and large fires were  $1.451$ ,  $2.165$ , and  $2.715 \text{ m/s}$ , as determined through iterative calculations.

**Table 3:** Vehicle type and heat release rate

Vehicle type	Maximum temperature ( $^{\circ}C$ )	Maximum heat release rate ( $MW$ )
Car	400–500	3–5
Bus or Railcar	700–800	15–20
Truck or tanker	1000–1200	50–100
Train	800–900	15–20

### 4.3 Smoke Diffusion Characteristics

Many scholars have studied the characteristics of smoke diffusion [36,37]. In this study, the entrance curve of a tunnel was examined. As mentioned in the previous section, the fire heat release rates were 5, 20, and 50 MW to simulate a small fire caused by a single car, a medium fire caused by a single bus, and a large fire caused by a single truck, respectively. The temperature distributions under different ventilation speeds were calculated. The longitudinal inlet flow velocity began at 0 m/s and was increased by 0.1 m/s until no smoke backflow occurred.

For a fire in the longitudinal section of the smoke temperature distribution in the center as a monitor, Figs. 15a and 15b show that when tunnel catches fire, a high-temperature smoke plume from the fire gathers at the top of the tunnel by buoyancy forces while spreading upstream and downstream. When there was no mechanical ventilation and the flow velocity was less than 1 m/s under natural ventilation conditions, high-temperature smoke only flowed in the tunnel vault and accumulated, exhibiting a good hierarchical structure. As the velocity of the incoming flow gradually increased, the layered structure at the top was destroyed by the shear action of the incoming flow. In Fig. 15c, the smoke layer in the downwind area of the fire source exhibited a wavy shape. As the ventilation velocity reached 1.5 m/s in Fig. 15d, the smoke backflow only occurred 1 m downstream of the source, and the backflow section was only 0.5-m long. The ventilation velocity at this time reached the critical velocity, and the high-temperature smoke no longer spread upstream to the fire source, which was conducive to the evacuation of people in the tunnel in the wind direction, and fire-fighters from upstream could move to the fire site to extinguish the fire out.

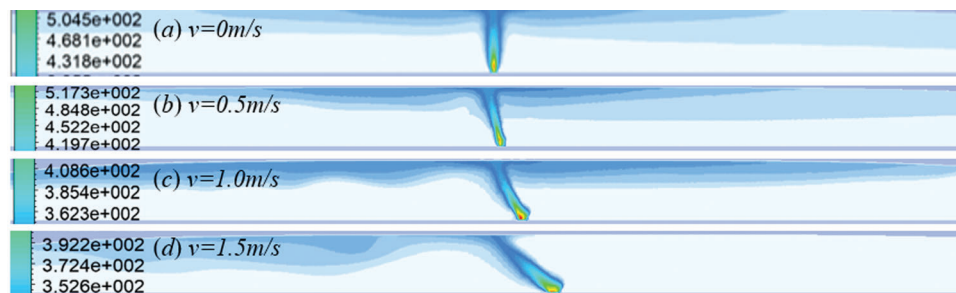


**Figure 15:** Distribution of smoke temperature under different ventilation velocities for a small fire in the curved section of the tunnel

The temperature and vertical velocity distribution on the center line of the tunnel sections upstream and downstream of the fire source were compared, as shown in Figs. 16 and 17. At the center of the tunnel and upstream of the fire source, as the longitudinal velocity increased, the air temperature near the vault equaled the temperature of the inflow. The longitudinal velocity near the vault gradually decreased from negative to

positive. Finally, the velocity distribution changed from a parabola at the bottom and a backflow at the top to a parabola across the whole tunnel section, which is similar to the velocity distribution of pipeline flow. At the center of the tunnel cross section and downstream of the fire source, the temperature at the top of the tunnel increased slightly with the increase in the velocity of the ventilation air. However, when the velocity reached the critical value, the maximum temperature occurred at a height near the center of the tunnel. In the direction downstream of the fire source, the longitudinal velocity exhibited a parabolic distribution in the lower part of the tunnel, while it surged at the top of the tunnel. The maximum velocity occurred near the vault.

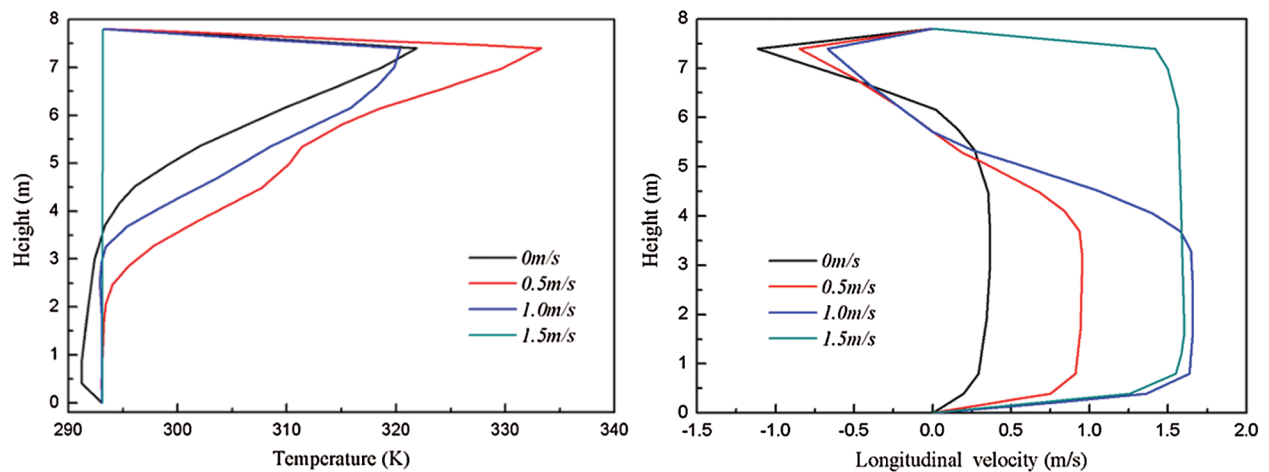


**Figure 16:** Temperature and longitudinal velocity distribution 5 m upstream of the fire source

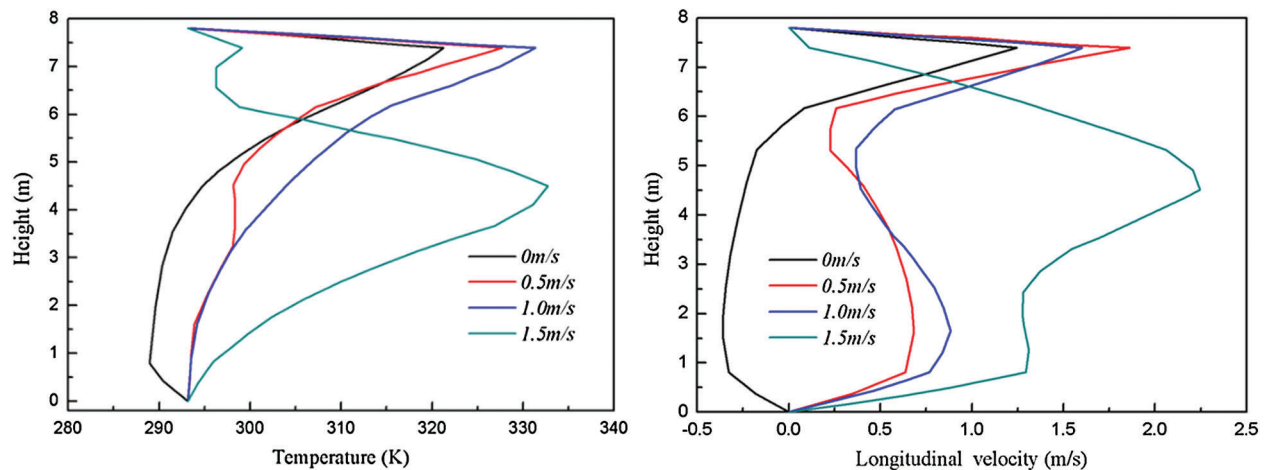


**Figure 17:** Temperature and longitudinal velocity distribution 5 m downstream of the fire source

The temperature distributions at different locations downstream of the tunnel fire under the critical velocity  $v = 1.5$  m/s are shown in Fig. 18. Five meters downstream of the fire source, due to the critical velocity, the structure of the smoke vortex was still relatively complete. The heat transfer due to convection was small, and the air temperature near the vault was high. Fifteen meters downstream of the fire source, as the vortex structure dissipated and buoyancy played a dominant role, the high-temperature smoke exhibited a stratified distribution across the tunnel cross section. Upon further diffusion of the

high-temperature smoke, the temperature distribution 35 m downstream of the fire source showed significant asymmetry. The temperature of the smoke outside the section was higher, while the temperature inside was lower. Sixty-five meters downstream of the fire source, the temperature stratification tended to be stable.

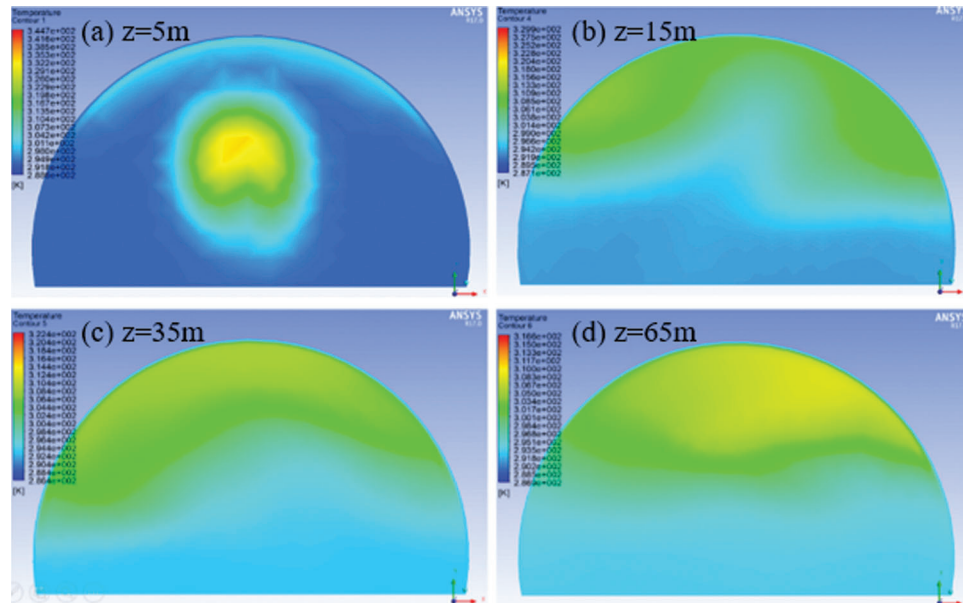


**Figure 18:** Temperature distribution at different locations downstream of the fire source. (a)  $z = 5$  m, (b)  $z = 15$  m, (c)  $z = 35$  m and (d)  $z = 65$  m

Based on Figs. 16–18, it was concluded that the smoke near the fire source diffused downstream in a symmetric vortex structure under the action of buoyancy, forming a vortex and drawing in a large amount of air. In this process, the movement of the smoke was a combination of a transverse vortex and longitudinal fluctuations. With the increase in the ventilation velocity, the temperature of the top layer near the fire source gradually decreased, and the maximum temperature point of the tunnel vault gradually moved back. When the critical velocity was reached, the spiral vortex structure of the high-temperature smoke flow generated by the fire source was relatively complete, the turbulent flow rate of the smoke was more severe, and it spread further downstream.

The fire conditions for different cases were calculated to obtain the critical velocities for different fire scales, as shown in Tab. 4. The critical velocities obtained through the numerical calculations were larger than those obtained by the theoretical calculations. Because a section of the tunnel was curved and affected by the curved wall boundary, the fluid inertia force was limited, and the buoyancy was more significant. The ratio of the buoyancy to the fluid inertia force represented by the Froude number ( $F_r$ ) was relatively large, and because  $F_r \propto v_c^{-1}$ , the theoretical calculation of the critical velocity was small.

**Table 4:** Critical velocity for fires of different sizes in the curved section

Fire scale		Small	Medium	Large
Heat release rate (MW)		5	20	50
Critical velocity (m/s)	Simulative velocity	1.5	2.4	3.1
	Theoretical velocity	1.451	2.165	2.715

Similarly, for the linear section in the middle of the tunnel, the fire heat release rates of 5, 20, and 50 MW were used to simulate a small fire of a single car (Fig. 19), a medium fire of a single bus, and a large fire of a single truck, respectively, and the temperature distributions for different ventilation speeds were analyzed. Fire conditions for the different cases were calculated to obtain the critical velocities of different fire scales, as shown in Tab. 5.

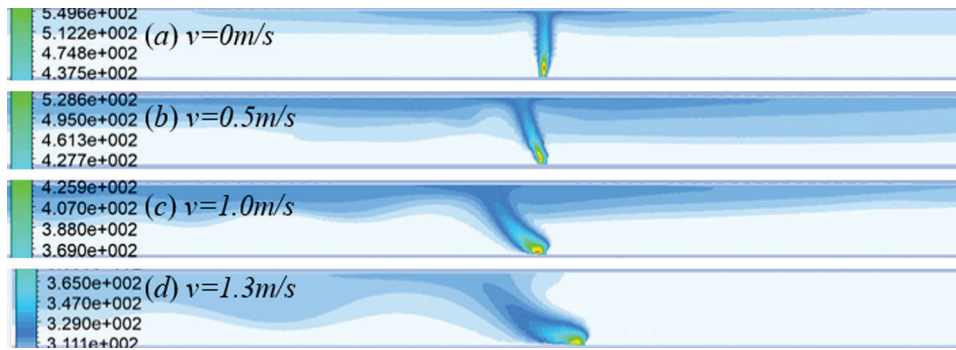


**Figure 19:** Distributions of smoke temperature for different velocities in small fire in linear section

**Table 5:** Critical velocities for fires of different sizes in the linear section

Fire scale	Small	Medium	Large
Heat release rate (MW)	5	20	50
Critical velocity (m/s)	Simulative velocity	1.4	2.6
	Theoretical velocity	1.451	2.165

The critical velocities obtained by the numerical simulations were slightly smaller than the theoretical values, but the overall growth was similar, and the difference did not exceed 0.2 m/s. Thus, the simulated and theoretical results were in good agreement. The simulated critical velocities of the curved and linear sections were compared with the theoretical values, as shown in Fig. 20.

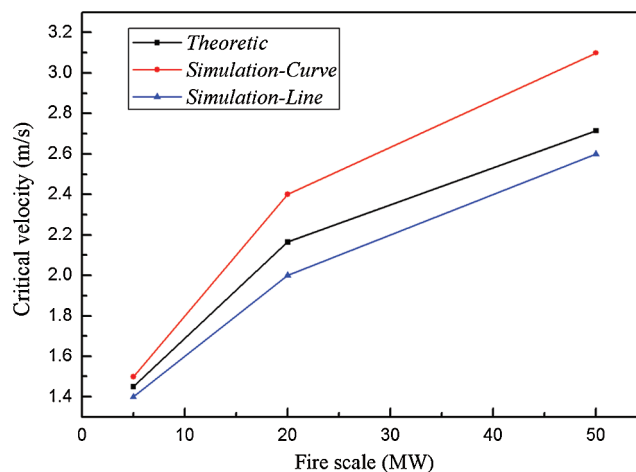


**Figure 20:** Theoretical and simulation values of the critical velocities

As shown in Fig. 20, when a fire occurred in the curved section, the critical velocity must be appropriately increased based on the theoretical value. When a fire occurs in a linear section, the theoretical critical velocity is sufficient to ensure that no smoke backflow occurs. Therefore, in the tunnel ventilation design, the fan pressurization in the curved section must be higher than that in the linear section.

#### 4.4 Evacuation from Tunnel Fire

##### 4.4.1 Escape Time

When a fire breaks out in the tunnel, the safe evacuation of people mainly depends on two time parameters: the required safety egress time (RSET) and the available safety egress time (ASET). When  $RSET < ASET$ , people in the tunnel can be evacuated safely during a fire. Otherwise, some people in the tunnel will be in danger. RSET can be calculated as follows:

$$RSET = t_1 + t_2 + t_3 \quad (9)$$

$t_1$  is the automatic fire alarm response time. According to regulations [38], the automatic fire alarm response time should not exceed 60 s, so  $t_1 = 60$  s.  $t_2$  is the time for people to move away from the burning vehicle after the fire alarm. Taking the 12-m-long bus in the worst-case scenario of full capacity as an example, the evacuation speed is about 0.2 m/s, and the time for people to leave their vehicles is 60 s. Thus,  $t_2$  was set to 60 s.  $t_3$  is the time for people to reach the safe area after getting off the bus. In the worst case, namely, congested conditions, the evacuation speed of people is 0.5 m/s, and the maximum distance for people to walk upstream and downstream is 150 m. Thus,  $t_3 = 300$  s. Therefore, the required safe evacuation time *REST* is  $60 \text{ s} + 60 \text{ s} + 300 \text{ s} = 420 \text{ s}$ .

##### 4.4.2 Analysis of Threat Degree during Evacuation

The critical dangerous state in a fire refers to the state in which the fire environment can cause severe injury to people. The critical state of a fire danger is determined by the following conditions:

- (1) When the interface of smoke layer is higher than the human eye height, and the temperature of the upper smoke layer reaches  $180^\circ\text{C}$ , there is a risk of people suffering radiation burns;
- (2) When the height of the flue gas layer is lower than the human eye height, and the temperature of flue gas reaches  $115^\circ\text{C}$ , there is a risk of people suffering direct burns.

In an environment where the temperature exceeds the body temperature, a person may experience dehydration due to sweating, exhaustion, and an accelerated heart rate. When the temperature exceeds  $66^\circ\text{C}$ , it becomes difficult to breathe. Consequently, it is difficult for firefighters to rescue people in the tunnel, and the evacuation of the tunnel is slowed.

The characteristic human eye height is 1.2–1.8 m. In this paper, the temperature 1.6 m from the ground of the evacuation channel (that is, the characteristic human eye height is 1.6 m) was taken as a criterion for the fire to reach a dangerous state. Furthermore, the upper limit of the safe temperature at a height of 1.6 m was set to  $60^\circ\text{C}$ . The time at which the temperature at a height of 1.6 m reached  $60^\circ\text{C}$  after the fire broke out was the available safe evacuation time (ASET). If  $ASET < RSET = 420$  s, people in the tunnel cannot escape safely.

There was a natural ventilation of 0.5–1 m/s in the tunnel, so under the conditions of 0.5 m/s, 1 m/s, and an open jet fan, the temperature distribution in the plane at a height of 1.6 m was simulated after 420 s for small, medium, and large fires. When the temperature along the evacuation route reached more than  $60^\circ\text{C}$ , it poses a threat to the evacuation of people in the tunnel.

If the tunnel is congested, people will follow the walls of the tunnel to escape. Fig. 21 shows the temperature distribution at the characteristic height of the human eye along the walls of the tunnel (ignoring the peak temperature at the fire source) when a single car burned. When a small fire occurred in

the tunnel, the maximum temperature at the human eye height in the tunnel did not reach 60°C (333 K) under natural ventilation. As the duration of the fire increased, the maximum temperature at the human eye height gradually increased, the location gradually migrated to the exit of the tunnel, and the amplitude gradually decreased. For general small fires, it was assumed that the full combustion phase lasted for 7 min, after which the temperature at the height of the human eye would not increase. Thus, there was no threat to the evacuating people during the whole fire duration.

When a medium-sized fire occurred (a single bus burned), the natural ventilation of 0.5 m/s was compared mechanical ventilation at the critical velocity. The results are shown in Fig. 22.

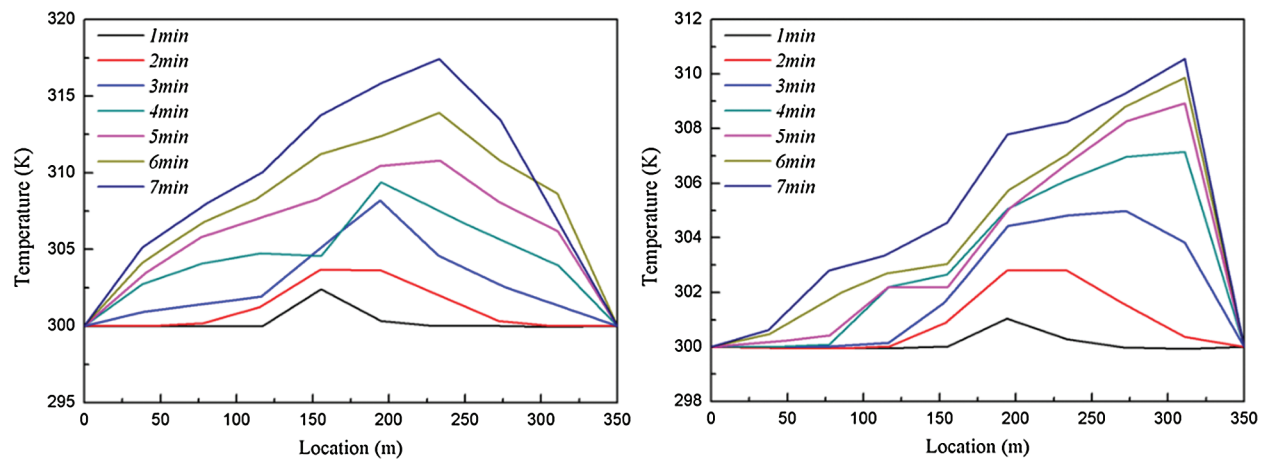


**Figure 21:** Temperature distribution at the characteristic human eye height for velocities of 0.5 m/s (left) and 1 m/s (right) with a small fire

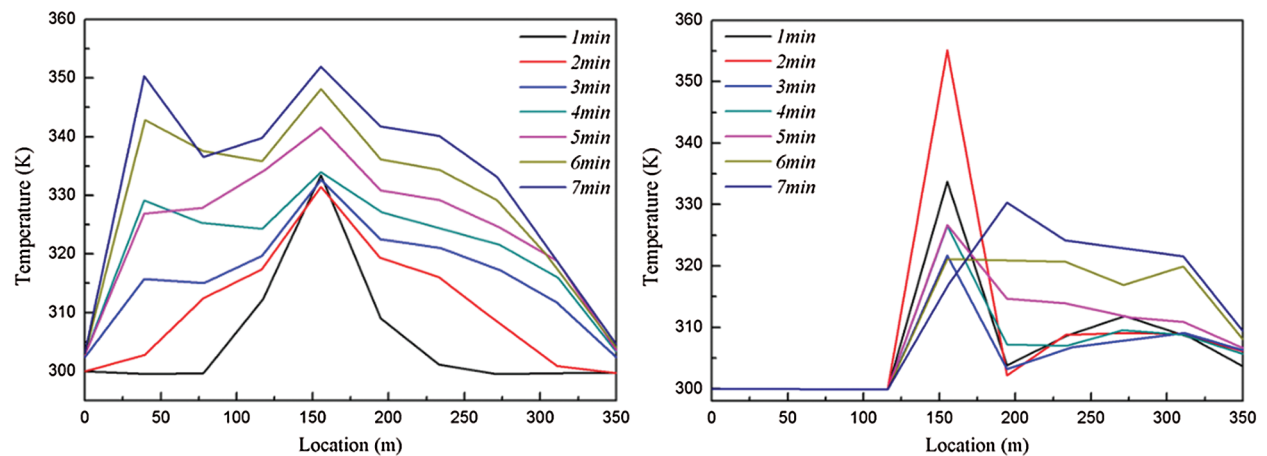


**Figure 22:** Temperature distribution at the characteristic human eye height at a velocity of 0.5 m/s (left) and the critical velocity (right) in a medium fire

Under natural ventilation, a point greater than 333 K appeared near the walls of the tunnel 10 m downstream of the fire source 4 min after the fire started. Thus, the evacuation of people in the tunnel would be endangered. At 5 min, the temperature from 40 m upstream to 35 m downstream of the fire source was above 333 K. If people were still stranded, it would be impossible to escape along the outer walls of the tunnel. As the fire continued, the maximum temperature gradually increased, and the

temperatures at more points in the tunnel exceeded the safe limit of 333 K. Six minutes after the fire, the temperatures 120 m upstream and 90 m downstream exceeded the safe limit, and basically the entire tunnel had no safe escape route.

If the jet fan was opened immediately, when the fire lasted for 1 min, the temperature 5 m downstream of the fire source reached 333 K. After, it expanded to a range from 10 m upstream to 20 m downstream within 1 min. When the fire lasted 3 min, the temperature in the entire tunnel was below 333 K, and people could escape in a safe state.

When a large-sized fire occurred (a single truck burned), the natural ventilation of 1.0 m/s and the mechanical ventilation at the critical velocity were compared. The result is shown in Fig. 23.

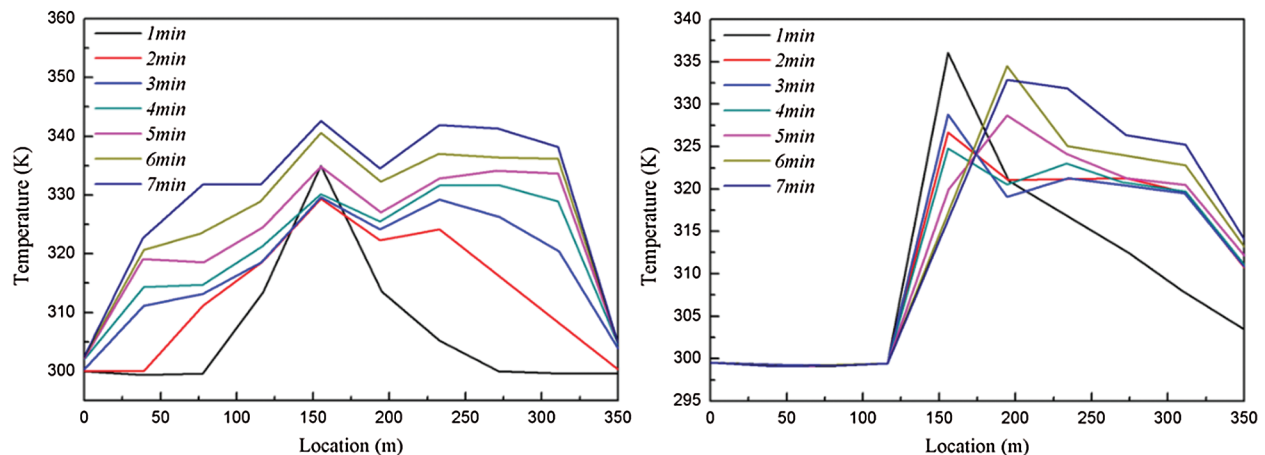


**Figure 23:** Temperature distribution at the characteristic human eye height at a velocity of 1.0 m/s (left) and the critical velocity (right) in a large fire

When the fire burned for 1 min, the temperatures 1–7 m upstream of the fire source point exceeded 333 K, and the highest temperature was 341 K. The safety of people in this range would be threatened, so it would be necessary to evacuate in time. Under the action of natural ventilation, the temperature in the tunnel was lower than 333 K, and people could escape quickly. When the fire lasted for 5 min, the temperature within 10 m downstream of the fire source and 50 m from the tunnel outlet were higher than 333 K. At this time, if there were still people who had not escaped, they would be harmed by the high temperature. When the fire lasted for 6 min, the temperature at the human eye height was higher than 333 K within the range from 30 m upstream to 120 m downstream of the fire source, making it difficult for people to escape from the fire safely.

If the jet fan opened immediately, when the fire lasted for 1 min, the temperature 2–15 m downstream of the fire source exceeded 333 K, which was unfavorable for evacuating the tunnel. However, in 2–5 min, the downstream temperature was lower than 333 K under the action of ventilation. After 6 min, under the influence of the jet fans, the temperature in the downstream 60–100 m exceeded 333 K, which was unfavorable for the safe evacuation of the tunnel.

## 5 Summary

The model created in this study was first compared with previously reported fire data for validation. The influence of the ventilation velocity on the smoke diffusion was simulated, and the critical velocity in the tunnel was calculated numerically when fires of different sizes occurred. The critical velocity value obtained using the Heselden & Kennedy formula was greater in the curved section, and the ventilation

needs were met in the straight section. Therefore, in the design of tunnel ventilation, the fan pressurization setting in the curved section should be higher than that in the linear section.

The threat degree to people evacuating a tunnel fire was also evaluated. The following results were obtained.

- (1) When a 5-MW fire occurred in the tunnel, the natural ventilation in the tunnel was sufficient, and the safety of people evacuating the tunnel would not be affected. For 20- or 50-MW fires in the tunnel, if only natural ventilation is used, the safety of the people in the tunnel will be affected. In this case, it is necessary to turn on mechanical ventilation to ensure the safe escape of people in the tunnel.
- (2) When a fire occurs in the tunnel and mechanical ventilation must be turned on, directly turning on mechanical ventilation will cause the fire smoke to spread rapidly downstream. This would be dangerous for people in the downstream region. Therefore, people escaping from downstream of the fire should evacuate within 5 min after the fire starts, and then the jet fan should be opened to suppress the adverse flow of smoke.

**Funding Statement:** This work is supported by the National Natural Science Foundation of China (Grant No. 11372166).

**Conflicts of Interest:** The authors declare that they have no conflicts of interest to report regarding the present study.

## References

1. Danziger, N. H. (1996). Fire life safety. *Tunnel Engineering Handbook*, pp. 369–383.
2. Tu, W. X. (1997). Experimental study on railway tunnel fire. *Fire Technology and Product Information*, 10, 32–36.
3. Bari, S., Naser, J. (2005). Simulation of smoke from a burning vehicle and pollution levels caused by traffic jam in a road tunnel. *Tunnelling and Underground Space Technology*, 20(3), 281–290. DOI 10.1016/j.tust.2004.09.002.
4. Hu, L. H., Huo, R., Li, Y. Z., Wang, H. B., Chow, W. K. (2005). Full-scale burning tests on studying smoke temperature and velocity along a corridor. *Tunnelling and Underground Space Technology*, 20(3), 223–229. DOI 10.1016/j.tust.2004.08.007.
5. Dennai, B., El, M., Khelifaoul, R. (2016). Numerical investigation of flow dynamic in mini- channel: case of a mini diode tesla. *Fluid Dynamics & Materials Processing*, 12(3), 102–110.
6. Ja, A., Cheddadi, A. (2017). Numerical simulation of thermosolutal convective transitions in a very narrow porous annulus under the influence of Lewis Number. *Fluid Dynamics & Materials Processing*, 13(4), 235–249.
7. Ihdene, M., Malek, T. B., Aberkane, S., Mouderes, M., Spiterri, P. et al. (2017). Analytical and numerical study of the evaporation on mixed convection in a vertical rectangular cavity. *Fluid Dynamics & Materials Processing*, 13(2), 85–105.
8. Triveni, M. K., Panua, R. (2018). Numerical study of natural convection in a right triangular enclosure with sinusoidal hot wall and different configurations of cold walls. *Fluid Dynamics & Materials Processing*, 14(1), 1–21.
9. Du, J., Wu, X., Li, R., Cheng, R. (2019). Numerical simulation and optimization of a mid-temperature heat pipe exchanger. *Fluid Dynamics & Materials Processing*, 15(1), 77–87. DOI 10.32604/fdmp.2019.05949.
10. Dobashi, M., Imai, T., Yanagi, H. H., Mizuno, A. (2000). Numerical simulation of the emergency tunnel ventilation for a tunnel with longitudinal and transverse systems combined. *BHR Group Conference Series*, pp. 581–596, USA.
11. Demouge, F., Lacroix, D., Gay, B. (2000). CFD simulation of fire smoke behaviour with transverse ventilation comparison with model tests. *BHR Group Conference Series*, pp. 615–628, USA.
12. Levy, S., Sandzimier, J. (2000). Smoke control for the ted Williams tunnel. *10th Int Symposium on Aerodynamics and Ventilation of Vehicle Tunnels*.
13. Yao, J. (2007). *On numerical simulation of temperature distribution in road tunnel fires (Master Thesis)*. Tongji University, China.
14. Wu, C., He, J., Ni, T. X. (2014). Research on the smoke movement in small radius curvilinear tunnel fires. *Fire Science and Technology*, 33(1), 37–40.

15. Wu, K. (2008). *Turbulent combustion modelling on long tunnel fires and structure fire safety (Ph.D. Thesis)*. Zhejiang University, China.
16. Hua, G. Y., Li, L., Yang, Z., Li, L. (2014). Boundary condition setting of tunnel fire simulation. *Heating Ventilating & Air Conditioning, 11*, 100–103.
17. Cao, Y. T. (2015). *Numerical simulation study of road tunnel fire danger under traffic congestion condition (Master Thesis)*. Anhui University of Science & Technology, China.
18. Good, G. M. L., Garry, K. P. (2004). On the use of reference models in automotive aerodynamics. SAE International, UK.
19. Zhang, Y. C. (2010). *Automotive wind tunnel corrections based on numerical simulation and test (Ph.D. Thesis)*. Jilin University, China.
20. Li, L. (2010). *Research on vehicle's transient aerodynamic characteristics at special running situations (Ph.D. Thesis)*. Shandong University, China.
21. Yuan, X. L. (2016). *Research on aerodynamic characteristics of vehicles driven out from tunnel under consistent crosswind (Master Thesis)*. Shandong University, China.
22. Xue, H., Ho, J. C., Cheng, Y. M. (2001). Comparison of different combustion models in enclosure fire simulation. *Fire Safety Journal, 36(1)*, 37–54. DOI 10.1016/S0379-7112(00)00043-6.
23. Huang, Y. L., Shiu, H. R., Chang, S. H., Wu, W. F., Chen, S. L. (2008). Comparison of combustion models in cleanroom fire. *Journal of Mechanics, 24(3)*, 267–275. DOI 10.1017/S172771910000232X.
24. Li, Z. Q. (2006). Application of discrete-ordinates model to the study of radiative heat transfer. *Journal of Aerospace Power, 21(2)*, 320–325.
25. Wang, Z. G. (2004). *CFD simulation and experimental research of gas-fired radiant heating (Master Thesis)*. Tianjin University, China.
26. Tan, Y. F. (2014). Numerical simulation of rotary self-cleaning air pre-filter based on CFD. *Acta Armamentarii, 35(3)*, 409–414.
27. He, F. X. (2016). Numerical analysis of air layer thickness of horizontally enclosed square cavity. *Journal of Shanghai Jiaotong University, 50(3)*, 384–388.
28. Massachusetts Highway Department, Brinckerhoff, P. (1995). *Memorial tunnel fire ventilation test program-test report*. Central Artery/tunnel Project, USA.
29. Martegani, A., Pavesi, G., Barbetta, C. (1997). The influence of separation, inclination and swirl on single and double jet fans installation efficiency. *BHR Group Conference Series*, pp. 43–55, Italy.
30. Li, H. H., Zhu, G. Q., Chen, S. S., Zhang, L., Zhang, J. (2011). Numerical simulation study on critical wind speed of the highway tunnel. *Fire Science and Technology, 30(3)*, 198–201.
31. Zhong, W., Duanmu, W. K., Wang, T., Liang, T. S. (2016). A study of the critical velocity of smoke bifurcation flow in tunnel with longitudinal ventilation. *Fire Technology, 53(2)*, 873–891. DOI 10.1007/s10694-016-0605-3.
32. Guo, X. J., Fang, C. P. (2018). Analysis of critical velocity in tunnel fire based on numerical simulation. *Sichuan Architecture, 38(1)*, 131–133.
33. Wang, S., Wang, Z. Y., Liang, Y., Wang, J. (2015). Simulation and analysis of smoke flow and personnel evacuation on a certain road tunnel in the fire. *Refrigeration & Air Conditioning, 29(4)*, 374–379.
34. Leitner, A. (2001). The fire catastrophe in the Tauern Tunnel: experience and conclusions for the Austrian guidelines. *Tunnelling and Underground Space Technology incorporating Trenchless Technology Research, 16(3)*, 217–223. DOI 10.1016/S0886-7798(01)00042-6.
35. Shi, X. Y., Yin, Q. C., Fang, N. (2014). A research to escape based on fire ventilation simulation analysis in highway tunnel. *Internet of Things Technologies, 4(6)*, 42–44+47.
36. Zhao, L. Y., Hu, F. L., Li, Q. (2019). Study on smoke propagation in subway tunnel with a fire scenario. *Software Guide, 18(1)*, 140–143.
37. Sánchez-Monroy, X., Mell, W., Torres-Arenas, J., Butler, B. W. (2019). Fire spread upslope: numerical simulation of laboratory experiments. *Fire Safety Journal, 108*, 102844. DOI 10.1016/j.firesaf.2019.102844.
38. JT/T 610–2004 (2004). Technical requirements for highway tunnel fire alarm equipment. CN-JT. <http://www.gov.cn/fuwu/bmfw/zggjzbzhglwyhgjbzxscx/index.html>.